

Lone-pair states as a key to understanding impact ionization in chalcogenide semiconductors

O Rubel and D Laughton

Thunder Bay Regional Research Institute, 290 Munro St, Thunder Bay, ON P7A 7T1, Canada
and
Lakehead University, 955 Oliver Road, Thunder Bay, ON P7B 5E1, Canada

E-mail: rubelo@tbh.net

Received 3 June 2010, in final form 7 June 2010

Published 13 August 2010

Online at stacks.iop.org/JPhysCM/22/355803

Abstract

Impact ionization of holes and domination of p-conductivity in chalcogenide semiconductors are attributed to a weak electron–phonon interaction inherent to lone-pair states. This argument is supported by first-principles calculations of an acoustical deformation potential in trigonal selenium. Results of the calculations reveal a strong dependence of the deformation potential on the excess energy of charge carriers. The latter is interpreted using a simple tight-binding model.

1. Introduction

It had long been believed that impact ionization was inherent to high-mobility crystalline semiconductors only, until it was found experimentally that amorphous selenium (a-Se) possesses impact ionization at practical electric fields [1–3]. This phenomenon has found an application in photosensors for high-sensitivity broadcasting camera tubes [2]. A combination of the unique photoconducting properties of a-Se with the effect of impact ionization has a high potential in x- and γ -ray detectors for medical imaging applications [4]. It is also believed that impact ionization is responsible for electrical switching between the crystalline and amorphous phases in Ge–Sb–Te alloys [5, 6]. The latter topic is being actively investigated in the context of new-generation non-volatile electronic data storage [7].

Experimental studies indicate that holes, not electrons, are responsible for impact ionization in a-Se [1] and $\text{Ge}_2\text{Sb}_2\text{Te}_5$ [5]. It is the presence of a chalcogen element that unites these two otherwise different materials. It is known that, if chalcogen is a major constituent in a semiconductor, the valence band in these materials is formed by unshared (lone-pair) electron states [8]. Since lone-pair states are not involved in chemical bonding, one can expect a response of the corresponding electronic states to a perturbation associated with phonons to be weak [9]. This may lead to a weaker electron–phonon interaction (and consequently a

weaker scattering) for holes in the lone-pair states as compared to electrons in anti-bonding states.

The purpose of this paper is to verify this hypothesis by performing first-principles calculations of an acoustical deformation potential in selenium. We will show that (i) the absolute value of the deformation potential for electrons exceeds that for holes, (ii) the deformation potential has a strong dependence on the excess energy of charge carriers and (iii) in the case of holes, this dependence is non-monotonic with a minimum at intermediate energies. Eventually, one can speculate that these observations favor the impact ionization of holes, which is in agreement with the experiments.

2. Calculation of the volume deformation potential

Here we limit our study to the interaction of charge carriers with long-wavelength acoustical phonons, thus leaving other scattering mechanisms beyond the scope of this paper. (However, it does not mean that other scattering mechanisms, i.e. optical phonon scattering, are irrelevant for high-field transport.) It is known from scattering theory that the rate of carrier scattering by phonons is proportional to the square of the deformation potential [10]. In the case of acoustic phonon scattering, the strength of the electron–phonon interaction is determined by a volume deformation potential.

Simulations of amorphous solids always entail some degree of structural uncertainty [11]. The structure of a-Se

consists of a mixture of chain and ring segments, the relative fraction of which is sensitive to deposition parameters [12–14]. For simplicity, we have chosen a crystalline structure of trigonal selenium (t-Se) for the purpose of our study under the assumption that the results obtained are also applicable to the amorphous phase. This choice is supported by x-ray, ultraviolet and inverse photoemission measurements [15–17] that reveal an almost identical density of states in amorphous and trigonal selenium. This is likely due to the fact that the amorphous structure preserves the equilibrium bond length and the bond angle on a short-range scale.

The unit cell of t-Se consists of three atoms, which leads to a total of nine phonon branches: three acoustical and six optical [18, 19]. One of the acoustical modes corresponds to the displacement of atoms along the chain (c axis). The other two modes are associated with the displacement of atoms in two directions perpendicular to the chain. In the following we calculate deformation potentials associated with such displacements.

Two deformation potentials, Ξ_{LA} and Ξ_{TA} , enter a matrix element for the interaction of charge carriers with longitudinal and transverse acoustical phonon modes, respectively. Taking a symmetry of the Brillouin zone into account, these deformation potentials can be expressed as [20]

$$\Xi_{LA} = \Xi_{\parallel} + (\Xi_{\perp} - \Xi_{\parallel}) \sin^2 \vartheta, \quad (1a)$$

$$\Xi_{TA} = \frac{1}{2}(\Xi_{\parallel} - \Xi_{\perp}) \sin 2\vartheta. \quad (1b)$$

Here Ξ_{\parallel} and Ξ_{\perp} are the deformation potentials associated with strain components parallel and perpendicular to the c axis, respectively, and ϑ is an angle between the phonon wavevector \mathbf{q} and the c axis. In the literature, strain-induced effects on the electronic structure are often expressed using Herring–Vogt deformation potentials. The parallel and perpendicular deformation potentials are related to dilatation and uniaxial deformation potentials in Herring–Vogt notation via $\Xi_d = \Xi_{\perp}$ and $\Xi_u = \Xi_{\parallel} - \Xi_{\perp}$, respectively.

Assuming that the distribution of ϑ 's is spherically symmetric (see [21], p 106), it can be eliminated from equation (1) by performing an averaging over $\sin \vartheta d\vartheta$. The result for the average squared longitudinal and transverse deformation potentials is

$$\langle \Xi_{LA}^2 \rangle = \Xi_{\parallel}^2 + \frac{4}{3}\Xi_{\parallel}(\Xi_{\perp} - \Xi_{\parallel}) + \frac{8}{15}(\Xi_{\perp} - \Xi_{\parallel})^2, \quad (2a)$$

$$\langle \Xi_{TA}^2 \rangle = \frac{2}{15}(\Xi_{\parallel} - \Xi_{\perp})^2. \quad (2b)$$

From comparison of the right-hand side in equation (2b) with the last term in equation (2a), it becomes apparent that scattering by longitudinal phonons will dominate. Next we calculate the deformation potentials Ξ_{\parallel} and Ξ_{\perp} in order to estimate $\langle \Xi_{LA}^2 \rangle$ for electrons and holes in t-Se.

By definition, the volume deformation potential Ξ_{Ω} is a proportionality factor between the relative change of the volume of a unit cell, Ω , and the strain-induced variation of an eigenvalue $E_n(\mathbf{k})$ specific to the band n and the vector \mathbf{k} in the Brillouin zone:

$$\delta E_n(\mathbf{k}) = \Xi_{\Omega,n}(\mathbf{k}) \frac{\delta \Omega}{\Omega}. \quad (3)$$

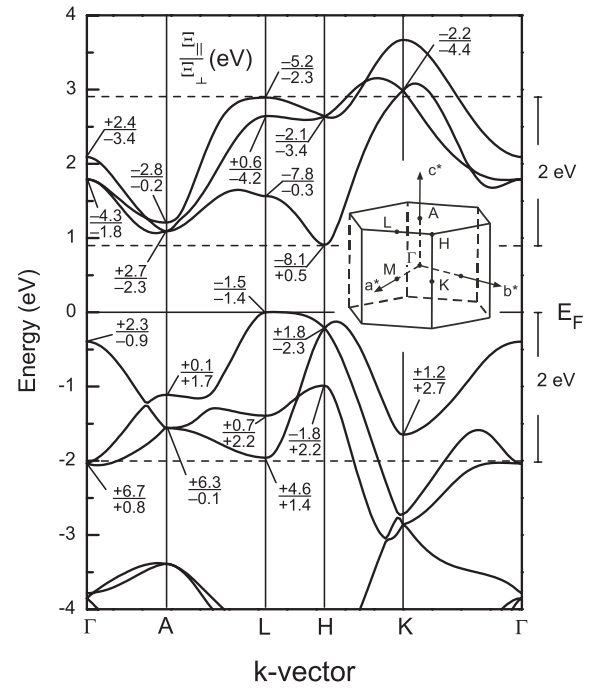


Figure 1. Band structure of trigonal selenium along some high-symmetry lines in the hexagonal Brillouin zone, which is shown in the inset. The deformation potentials Ξ_{\parallel} (eV) due to the uniaxial strain ϵ_{zz} and Ξ_{\perp} (eV) due to the biaxial strain $\epsilon_{xx} = \epsilon_{yy}$ are indicated for selected \mathbf{k} -points in 2 eV energy windows.

The deformation potential can be found by comparing the electronic structure of strained and unstrained atomic models calculated using a density functional theory (DFT).

Calculations of the electronic structure were performed using a full-potential linearized augmented plane-wave method implemented in the WIEN2K package [22] and a local density approximation [23] for the exchange–correlation functional. The volume of a cell was partitioned onto nonoverlapping spheres with a radius of 2 Bohr centered at the nucleus of individual atoms. The energy to separate core and valence electrons was set to -6 Ryd. The product of the atomic sphere radius and plane-wave cutoff in k -space (the so-called RKmax parameter) was equal to 7. The Brillouin zone of a primitive unit cell was sampled using a $10 \times 10 \times 8$ Monkhorst–Pack mesh [24]. The selected parameters provide an adequate convergence of the calculated deformation potential.

The absolute deformation potential Ξ_{\parallel} due to a uniaxial strain ϵ_{zz} along the helical chain was calculated using a supercell approach [25]. This method, however, is compatible with uniaxial strain only. Therefore, when calculating the deformation potential Ξ_{\perp} due to the volume expansion in a plane perpendicular to the c axis, we took the energy level of the 1s core state as a reference, assuming that it is not sensitive to the volume deformation. The latter approach was successfully applied to the calculation of volume deformation potentials in III–V and II–VI semiconductors [26]. The systematic error introduced by this approximation into the calculated value of the deformation potential is about 1 eV.

Figure 1 illustrates the dependence of the deformation potentials Ξ_{\parallel} and Ξ_{\perp} on the \mathbf{k} -vector for high-symmetry

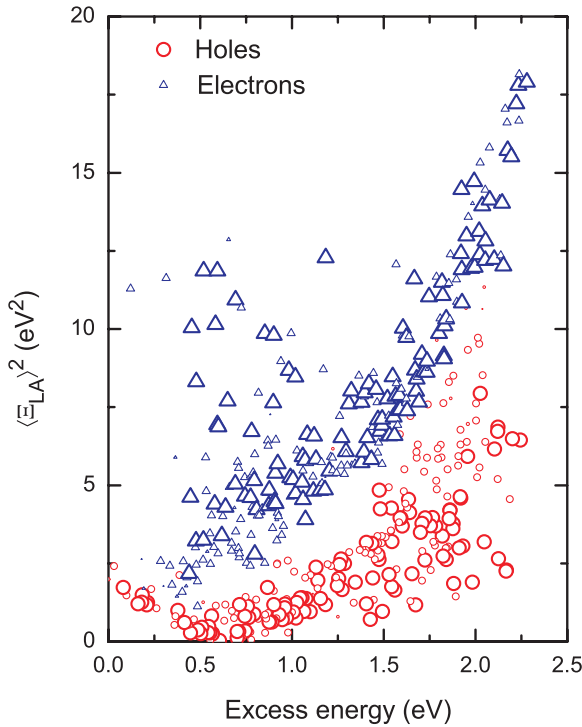


Figure 2. Dependence of the average longitudinal acoustical deformation potential defined by equation (2a) on the excess energy for electrons and holes. The excess energy for electrons and holes is measured from the bottom of the conduction band at the H-point and the top of the valence band at the L-point, respectively. The size of the symbols is proportional to the weight of a particular \mathbf{k} -point. (This figure is in colour only in the electronic version)

directions of the Brillouin zone. The conduction band minima (H valley) has the highest absolute value of the deformation potential and is mostly sensitive to longitudinal deformations. The absolute value of the deformation potential for the valence band maximum (L valley) is comparatively low (only 1.5 versus 8.1 eV for the conduction band).

Being accelerated by the applied electric field, carriers have enough kinetic energy to span the entire Brillouin zone. Therefore, we calculated the longitudinal deformation potential $\langle \Xi_{LA}^2 \rangle$ in 94 k -points evenly spread in the irreducible Brillouin zone. The result as a function of the excess energy of a charge carrier is illustrated in figure 2. The size of symbols in figure 2 represents the weight of a particular \mathbf{k} -point, i.e. the number of equivalent \mathbf{k} -points in the Brillouin zone.

3. Discussion

In spite of the scattering of data in figure 2, the following trends can be noticed: (i) a parabolic dependence of $\langle \Xi_{LA}^2 \rangle$ on the excess energy of holes with a minimum at the hole energies of about 0.4–0.8 eV, (ii) overall, much higher deformation potentials for electrons than for holes and (iii) an increase of the deformation potential as the excess energy approaches the ionization threshold, which is about 2 eV. These features will be interpreted below in terms of a simple tight-binding model [27].

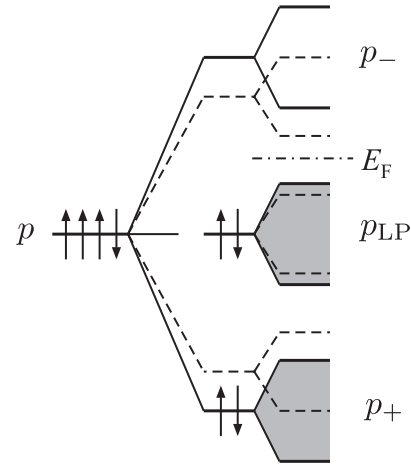


Figure 3. Effect of the volume expansion on the energy bands in trigonal selenium (schematic). Solid and dashed lines correspond to the energy levels in the unstrained and strained lattice, respectively. E_F is the Fermi energy.

Six valence electrons ($4s^2 4p^4$) per atom in selenium favor a chain structure in which every atom has two neighbors. The doubly occupied s states lie deep in energy and their admixture to p states is low [14]. The valence and conduction bands are formed essentially by p states. The hybridization splits atomic p states into bonding p_+ , anti-bonding p_- and lone-pair p_{LP} states as illustrated in figure 3. The remaining four valence electrons occupy p_+ and p_{LP} states. Thus, the bottom of the conduction band and the top of the valence band are associated with p_- and p_{LP} states, respectively [8].

Splitting of the energy levels and the bandwidth are determined by a mutual orientation of p orbitals in adjacent atoms and interatomic matrix elements $V_{pp\sigma}$ and $V_{pp\pi}$. These matrix elements depend on the interatomic spacing as d^{-2} (see [28], p 48), which is a primary source for the volume deformation potential. A uniform volume expansion reduces both $|V_{pp\sigma}|$ and $|V_{pp\pi}|$ that results in a shift of p_+ and p_- bands towards one another and, simultaneously, a shrinking of all bands (see figure 3, dashed lines). Apparently, the states in the middle of the lone-pair band are least affected by the strain, which qualitatively agrees with the results in figure 2.

The energy dependence of the deformation potential will have consequences for the mean free path due to scattering by phonons, since the latter is inversely proportional to the square of the deformation potential. The mean free path for holes will get longer as their kinetic energy increases, while for electrons we expect the opposite dependence. This observation is in line with an empirical finding of Kasap *et al* [29], who had to imply an increase in the mean free path of holes as their excess energy increases in order to fit experimental data for the field dependence of the impact ionization coefficient in a-Se.

Finally, we can apply this discussion to interpretation of high-field transport phenomena in other chalcogenides and their alloys in which the valence band is formed by lone-pair states. A prominent example is an electronic switching observed in a variety of crystalline and non-crystalline chalcogenide semiconductors [30]. For instance,

studies of the current–voltage characteristic for amorphous $\text{Ge}_2\text{Sb}_2\text{Te}_5$ show an abrupt transition from a low-conducting to a high-conducting state while passing over some critical value of the bias [5]. Analyzing these data, Pirovano *et al* [5] suggested the impact ionization of holes as a possible cause for the observed switching between two conducting states, which has also been supported by later theoretical studies [6]. In light of the preceding discussion, we can attribute a dominant p-type conductivity [31] and the avalanche of holes in these materials to the weak electron–phonon interaction inherent to lone-pair states.

4. Conclusion

Since the lone-pair states are not involved in bonding, their response to the volume deformation associated with acoustical phonons is low compared to the conduction band formed by anti-binding states. We preliminarily link these results with the favorable high-field transport of holes in chalcogenide semiconductors corroborated by experimental observations of impact ionization in amorphous selenium and electronic switching in Ge–Sb–Te alloys. However, in order to make this conclusion unambiguous, more detailed study is necessary, which will include optical phonons, effects of the density of states and a wavefunction overlap on the matrix element for electron–phonon coupling.

Acknowledgments

Financial support of the Thunder Bay Regional Health Sciences Foundation and of the Natural Sciences and Engineering Council of Canada (discovery grant 386018-2010) is gratefully acknowledged.

References

- [1] Juska G and Arlauskas K 1980 *Phys. Status Solidi* a **59** 389
- [2] Tanioka K, Yamazaki J, Shidara K, Taketoshi K, Kawamura T, Ishioka S and Takasaki Y 1987 *IEEE Electron Device Lett.* **8** 392
- [3] Tsuji K, Takasaki Y, Hirai T and Taketoshi K 1989 *J. Non-Cryst. Solids* **114** 94
- [4] Reznik A, Baranovskii S D, Rubel O, Jandieri K, Kasap S, Ohkawa Y, Kubota M, Tanioka K and Rowlands J 2008 *J. Non-Cryst. Solids* **354** 2691
- [5] Pirovano A, Lacaíta A L, Benvenuti A, Pellizzer F and Bez R 2004 *IEEE Trans. Electron Devices* **51** 452
- [6] Jandieri K, Rubel O, Baranovskii S D, Reznik A, Rowlands J A and Kasap S O 2009 *J. Mater. Sci., Mater. Electron.* **20** S221
- [7] Wuttig M and Yamada N 2007 *Nat. Mater.* **6** 824
- [8] Kastner M 1972 *Phys. Rev. Lett.* **28** 355
- [9] Baranovskii S, Bordovskii G, Kazakova L, Lebedev E, Lyubin V and Savinova N 1984 *Sov. Phys.—Semicond.* **18** 633
- [10] Seeger K 2004 *Semiconductor Physics: An Introduction* 9th edn (Berlin: Springer)
- [11] Drabold D A 2009 *Eur. Phys. J. B* **68** 1
- [12] Misawa M and Suzuki K 1978 *J. Phys. Soc. Japan* **44** 1612
- [13] Kaplow R, Rowe T A and Averbach B L 1968 *Phys. Rev.* **168** 1068
- [14] Joannopoulos J D, Schlüter M and Cohen M L 1975 *Phys. Rev. B* **11** 2186
- [15] Shevchik N J, Tejada J, Cardona M and Langer D W 1973 *Solid State Commun.* **12** 1285
- [16] Shevchik N J, Cardona M and Tejada J 1973 *Phys. Rev. B* **8** 2833
- [17] Ono I, Grekos P C, Kouchi T, Nakatake M, Tamura M, Hosokawa S, Namatame H and Taniguchi M 1996 *J. Phys.: Condens. Matter* **8** 7249
- [18] Teuchert W D and Geick R 1974 *Phys. Status Solidi* b **61** 123
- [19] Teuchert W D, Geick R, Landwehr G, Wendel H and Weber W 1975 *J. Phys. C: Solid State Phys.* **8** 3725
- [20] Bir G L and Pikus G E 1972 *Symmetry and Strain-Induced Effects in Semiconductors* (Moscow: Nauka) (in Russian)
- [21] Conwell E M 1967 *High Field Transport in Semiconductors (Solid State Physics: Advances in Research and Applications)* (New York: Academic)
- [22] Blaha P, Schwarz K, Madsen G K H, Kvasnicka D and Luitz J 2001 *Wien2k: An Augmented Plane Wave + Local Orbitals Program for Calculating Crystal Properties* Karlheinz Schwarz, Techn. Universität Wien, Austria
- [23] Perdew J P and Wang Y 1992 *Phys. Rev. B* **45** 13244
- [24] Monkhorst H J and Pack J D 1976 *Phys. Rev. B* **13** 5188
- [25] Van de Walle C G and Martin R M 1989 *Phys. Rev. Lett.* **62** 2028
- [26] Wei S-H and Zunger A 1999 *Phys. Rev. B* **60** 5404
- [27] Reitz J R 1957 *Phys. Rev.* **105** 1233
- [28] Harrison W A 1989 *Electronic Structure and Properties of Solids* (New York: Dover)
- [29] Kasap S, Rowlands J A, Baranovskii S D and Tanioka K 2004 *J. Appl. Phys.* **96** 2037
- [30] Ovshinsky S R 1968 *Phys. Rev. Lett.* **21** 14503
- [31] Mott N F and Davis E A 1971 *Electronic Processes in Non-Crystalline Materials* (Oxford: Clarendon)